



Macraeite, [(H₂O)K]Mn₂(Fe₂Ti)(PO₄)₄[O(OH)](H₂O)₁₀ · 4H₂O, a new monoclinic paulkerrite-group mineral, from the Cubos–Mesquitela–Mangualde pegmatite, Portugal

Ian E. Grey¹, Christian Rewitzer², Rupert Hochleitner³, Anthony R. Kampf⁴, Stephanie Boer⁵,
William G. Mumme¹, and Nicholas C. Wilson¹

¹CSIRO Mineral Resources, Private Bag 10, Clayton South, Victoria 3169, Australia

²independent researcher: Graf von Bogen Str. 6, 93437 Furth im Wald, Germany

³Bavarian State Collection for Mineralogy (SNSB), Theresienstrasse 41, 80333 Munich, Germany

⁴Mineral Sciences Department, Natural History Museum of Los Angeles County, 900 Exposition Boulevard,
Los Angeles, CA 90007, USA

⁵Australian Synchrotron, 800 Blackburn Road, Clayton, Victoria 3168, Australia

Correspondence: Ian E. Grey (ian.grey@csiro.au)

Received: 28 November 2023 – Revised: 30 December 2023 – Accepted: 31 January 2024 – Published: 13 March 2024

Abstract. Macraeite, [(H₂O)K]Mn₂(Fe₂Ti)(PO₄)₄[O(OH)](H₂O)₁₀ · 4H₂O, is a new monoclinic member of the paulkerrite group, from the Cubos–Mesquitela–Mangualde pegmatite, Mangualde, Portugal. It was found in phosphate nodules of weathered triplite, heterosite, and lithiophilite. Associated minerals are strengite, triplite, bermanite, phosphosiderite, and switzerite.

Macraeite forms colourless to light-greenish-yellow pseudo-rhombic dodecahedral-shaped crystals up to 0.15 mm. The crystals are equant with forms {010}, {001}, {111}, and { $\bar{1}11$ }. The calculated density is 2.39 g cm⁻³. Optically, macraeite crystals are biaxial (+), with $\alpha = 1.605(3)$, $\beta = 1.611(3)$, $\gamma = 1.646(3)$ (measured in white light), and $2V(\text{meas}) = 45(3)^\circ$. The empirical formula from electron microprobe analyses and structure refinement is $A^1[(\text{H}_2\text{O})_{0.83}\text{K}_{0.17}]_{\Sigma 1.00} A^2[\text{K}_{0.65}(\text{H}_2\text{O})_{0.35}]_{\Sigma 1.00} M^1(\text{Mn}_{1.98}^{2+}\square_{0.02})_{\Sigma 2.00} M^2(\text{Fe}_{1.09}^{3+}\text{Al}_{0.31}\text{Ti}_{0.52}^{4+}\text{Mg}_{0.08})_{\Sigma 2.00} M^3(\text{Ti}_{0.66}^{4+}\text{Fe}_{0.34}^{3+})_{\Sigma 1.00} (\text{PO}_4)_4 X[\text{O}_{0.87}\text{F}_{0.53}(\text{OH})_{0.60}]_{\Sigma 2.00} (\text{H}_2\text{O})_{10} \cdot 4\text{H}_2\text{O}$.

Macraeite has monoclinic symmetry with space group $P2_1/c$ and unit-cell parameters $a = 10.562(2)$ Å, $b = 20.725(4)$ Å, $c = 12.416(2)$ Å, $\beta = 90.09(3)^\circ$, $V = 2717.8(9)$ Å³, and $Z = 4$. The crystal structure was refined using synchrotron single-crystal data to $wR_{\text{obs}} = 0.065$ for 4990 reflections with $I > 3\sigma(I)$. Macraeite is isostructural with the paulkerrite-group minerals rewitzerite and paulkerrite, with ordering of K and H₂O at different A sites ($A1$ and $A2$) of the general formula $A1A2M1_2M2_2M3(\text{PO}_4)_4X_2(\text{H}_2\text{O})_{10} \cdot 4\text{H}_2\text{O}$, whereas in the orthorhombic member, benyacrite, K and H₂O are disordered at a single A site.

1 Introduction

The Cubos–Mesquitela–Mangualde pegmatite formation, Portugal, is an important locality for secondary phosphate minerals, with Mindat listing 107 valid minerals reported from the locality of which 67 are phosphates, including the three type-locality minerals jahnsite-(CaMnMn), rittmanite, and zodacite. No minerals of the paulkerrite group

(Peacor et al., 1984; Fransolet et al., 1984; Demartin et al., 1997; Grey et al., 2023a) have been reported from this locality, although members of the group have been reported from the nearby Folgosinho pegmatite (Keck et al., 1998; Schnorrer and Tetzner, 2005). Specimens of phosphate nodules collected by one of the authors (Christian Rewitzer) from the Mangualde pegmatite mine dump were re-

cently analysed using scanning electron microscopy (SEM), energy-dispersive X-ray analysis and powder X-ray diffraction (XRD) and were found to contain crystals of a mineral belonging to the paulkerrite group. More detailed studies on the Mangualde specimens, involving electron microprobe analyses and single-crystal XRD, confirmed that the crystals corresponded to a new species, the Fe analogue of the monoclinic paulkerrite-group member rewitzerite, $\text{K}(\text{H}_2\text{O})\text{Mn}_2(\text{Al}_2\text{Ti})(\text{PO}_4)_4[\text{O}(\text{OH})](\text{H}_2\text{O})_{10} \cdot 4\text{H}_2\text{O}$ (Grey et al., 2023b), with Fe replacing Al. The mineral and its name have been approved by the International Mineralogical Association (IMA) Commission on New Minerals, Nomenclature and Classification (CNMNC), IMA-2023-065.

The name honours Colin MacRae (born 1961) for his important contributions to the characterisation of new mineral species using electron microprobe techniques. Since 2010, he has conducted electron microprobe analyses on 40 minerals, all of which were approved as new mineral species. As head of the Microbeam Laboratory at CSIRO Mineral Resources, Clayton, Victoria, Australia, he has been responsible for the development of new techniques that are of benefit to the analysis of highly hydrated, beam-sensitive secondary minerals. This includes the integration of liquid nitrogen cold-stage technology into the electron microprobe to reduce beam damage and modifications to the raw-data processing software to include water in the matrix correction. Colin MacRae has given his permission for the mineral name.

The holotype specimen is housed in the mineralogical collections of the Natural History Museum of Los Angeles County, catalogue number 76293. A co-type, from which the images in Figs. 1 to 3 were taken, is in the Bavarian State Collection for Mineralogy, Munich, registration number MSM 38050.

2 Occurrence and associated minerals

The locality for macraeite is a phosphate pegmatite within a pegmatite formation now called Cubos–Mesquitela–Mangualde. It is located near the village of Mesquitela close to Mangualde, in the district of Viseu in the northern centre of Portugal ($40^\circ 35' 13.7'' \text{N}$, $7^\circ 45' 04.3'' \text{W}$). A mining concession at the pegmatite, Chão do Castanheiro, has been operated by the Carolino family since 1935, mining for quartz and feldspar and also Be, Li, and Ta. Specimens containing macraeite were collected in 1984 on the dumps of the mine site. The specimens were in the form of phosphate nodules of weathered triplite, heterosite, and lithiophilite. Associated minerals are deep reddish-purple crystals of strengite, tan deeply etched triplite, reddish-brown bermanite, inky-blue phosphosiderite, and occasional switzerite.

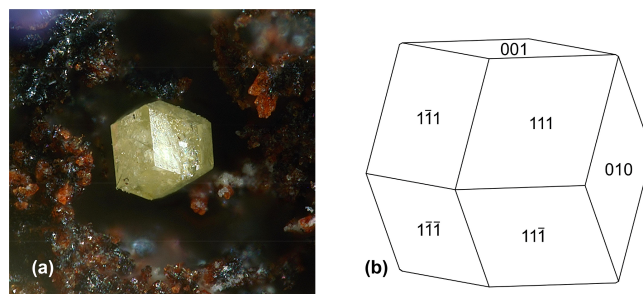


Figure 1. (a) Isolated crystal of macraeite associated with red-brown bermanite on specimen MSM38050. Field of view (FOV) 0.55 mm. Photo by Christian Rewitzer. (b) Crystal drawing of macraeite. Clinographic projection.



Figure 2. Macraeite crystals associated with red-brown bermanite and purple strengite on specimen MSM38050. FOV 1.3 mm. Photo by Christian Rewitzer.

3 Physical and optical properties

Macraeite occurs as light-greenish-yellow equant euhedral crystals with relatively uniform sizes from sub-100 to $\sim 150 \mu\text{m}$. Individual crystals have a pseudo-rhombic dodecahedral shape (Fig. 1) although the crystals are more commonly aggregated and form complex intergrowths (Figs. 2, 3) with dimensions of up to 0.5 mm. The crystal forms are $\{010\}$, $\{001\}$, $\{111\}$, and $\{\bar{1}\bar{1}\bar{1}\}$ as shown in Fig. 1. The calculated density, for the empirical formula and single-crystal unit-cell volume, is 2.39 g cm^{-3} .

Optically, macraeite crystals are biaxial (+), with $\alpha = 1.605(3)$, $\beta = 1.611(3)$, and $\gamma = 1.646(3)$ (measured in white light). The measured $2V$ from extinction data analysed with EXCALIBR (Gunter et al., 2004) is $45(3)^\circ$, and the calculated $2V$ is 25.8° . Dispersion is strong with $r < v$. The optical orientation is $X = b$, $Y = c$, $Z = a$. The Gladstone–Dale

Table 1. Analytical data (wt %) for macraeite.

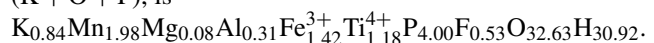
Constituent	Mean	Range	SD	Standard
K ₂ O	4.14	3.70–4.89	0.37	Adularia
MnO	14.63	13.33–15.91	0.86	MnSiO ₃
MgO	0.35	0.21–0.55	0.12	Spinel
Al ₂ O ₃	1.65	0.23–3.68	0.96	Berlinite
Fe ₂ O ₃	11.80	10.24–13.66	0.86	Hematite
TiO ₂	9.85	8.65–11.10	0.83	Rutile
P ₂ O ₅	29.55	26.20–32.01	2.20	Berlinite
F	1.04	0.39–2.03	0.47	Fluorite
H ₂ O _{calc}	28.90			
–O ≡ F	–0.44			
Total	101.47			

compatibility index (Mandarino, 1981) is 0.020 (excellent) based on the empirical formula and the calculated density.

4 Chemical composition

Crystals of macraeite were analysed using wavelength-dispersive electron microprobe (EMP) spectrometry on a JEOL JXA-8500F Hyperprobe operated at an accelerating voltage of 15 kV and a beam current of 2.2 nA. The beam was defocused to 10 μm. Analytical results (average of 17 analyses on 17 crystals) are given in Table 1. There was insufficient material for direct determination of H₂O, so it was based upon the crystal structure. The analyses were affected by dehydration of the specimen in the high vacuum of the microprobe. The dehydration was accompanied by strong cracking of the crystals, as shown in Fig. 3. This resulted in increasing analysis totals with increasing time in the vacuum. The totals shown in Table 1 cover the range 96.4 to 108.8. This behaviour is common to highly hydrated paulkerrite-group minerals, as noted by Sejkora et al. (2006), who reported EMP analysis totals in the range of 115 % to 119 % for their analyses of benyacarite.

The empirical formula, normalised to 4P and 34 (K + O + F), is



The least-squares programme OccQP (Wright et al., 2000) was used to obtain optimised site assignments for the *M1* to *M3* sites based on the refined bond distances and site scattering and the chemical analyses, giving the empirical formula in structural form as $A^1[(\text{H}_2\text{O})_{0.83}\text{K}_{0.17}]_{\Sigma 1.00} A^2[\text{K}_{0.65}(\text{H}_2\text{O})_{0.35}]_{\Sigma 1.00} M^1(\text{Mn}_{1.98}^{2+})_{\Sigma 2.00} M^2(\text{Fe}_{1.09}^{3+}\text{Al}_{0.31}\text{Ti}_{0.52}^{4+}\text{Mg}_{0.08})_{\Sigma 2.00} M^3(\text{Ti}_{0.66}^{4+}\text{Fe}_{0.34}^{3+})_{\Sigma 1.00} (\text{PO}_4)_4 X[\text{O}_{0.87}\text{F}_{0.53}(\text{OH})_{0.60}]_{\Sigma 2.00} (\text{H}_2\text{O})_{10} \cdot 4\text{H}_2\text{O}$, where the *A*-site occupancies are from the structure refinement.

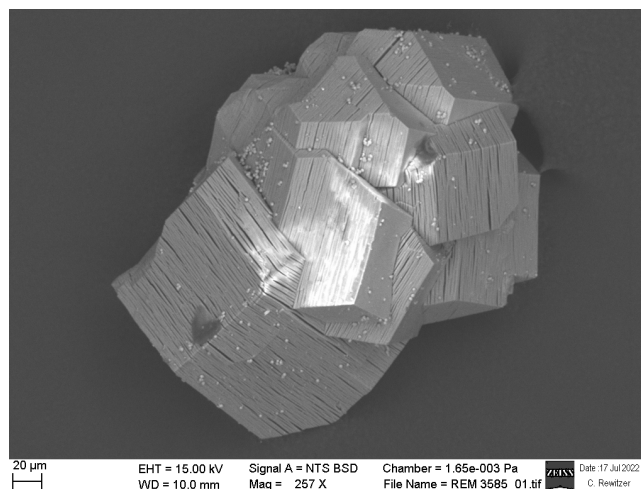
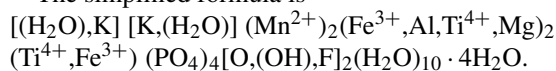


Figure 3. Scanning electron microscope back-scattered electron image of intergrown macraeite crystals, showing crystallographically controlled parallel cracking due to dehydration in the microscope vacuum.

The simplified formula is



The ideal end-member formula based on the dominant constituents at each site is $[(\text{H}_2\text{O})\text{K}]\text{Mn}_2(\text{Fe}_2\text{Ti})(\text{PO}_4)_4[\text{O}(\text{OH})](\text{H}_2\text{O})_{10} \cdot 4\text{H}_2\text{O}$, which requires K₂O 4.75, MnO 14.31, Fe₂O₃ 16.11, TiO₂ 8.06, P₂O₅ 28.63, and H₂O 28.14, with total 100 wt %.

Note that the (OH) is only marginally higher than F in the empirical formula calculated from the mean F content. The individual F analyses span a wide range from 0.39 wt % to double the mean F content. The higher-F analyses would give F > OH in the empirical formula, corresponding to a fluor-macraeite.

The empirical formula shows considerable mixing of the major constituents, Ti and Fe³⁺, between the crystallographically similar *M2* and *M3* sites such that changes in the location of minor constituents between the sites can change the dominant constituents. This problem is common to paulkerrite-group minerals, and to overcome it the compositions at the *M2* and *M3* sites are merged and an unambiguous end-member can be obtained using the site-total-charge method (Bosi et al., 2019a, b). This approach has been approved by the IMA CNMNC, revised proposal 22-K-bis. It is illustrated for macraeite in Fig. 4, which shows possible end-member compositions and their phase-fields based on occupation of the merged (*M2M3*) sites by Al, Ti, and Fe³⁺. For macraeite, the composition at the merged sites is $M^{2+M3}(\text{Fe}_{1.43}^{3+}\text{Ti}_{1.18}\text{Al}_{0.31}\text{Mg}_{0.08})$. Removing the minor amount of Mg and scaling to 3(Fe³⁺ + Ti + Al) gives Fe_{1.46}Ti_{1.22}Al_{0.32}. This composition, shown by the cross in Fig. 4, sits in the Fe₂Ti end-member compositional field. Thus, for macraeite, the dominant-constituent

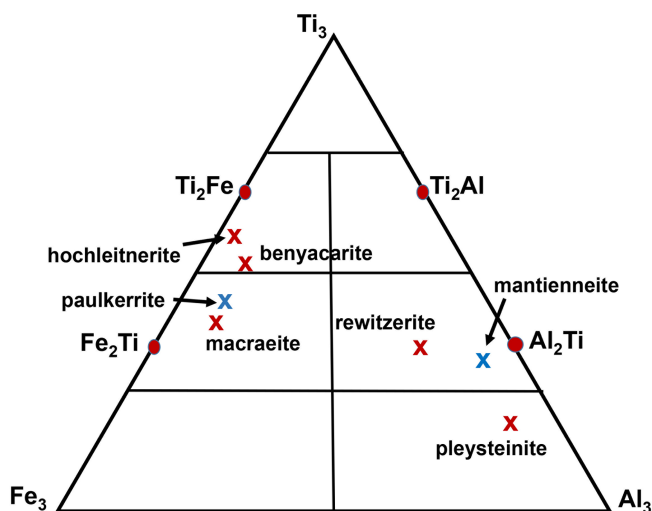


Figure 4. Ternary diagram for $(M2)_2M3$ site Al–Ti–Fe³⁺ compositions, showing end-member compositions (Al₂Ti, Ti₂Al, etc.) and location of the empirical composition for macraeite. For comparison, the published empirical compositions are shown for the paulkerrite-group minerals benyacarite (Demartin et al., 1997), paulkerrite (Peacor et al., 1984), mantienneite (Fransolet et al., 1984), rewtizerite (Grey et al., 2023b), pleysteinite (Grey et al., 2023c), and hochleitnerite (Grey et al., 2023d). Red crosses correspond to minerals with Mn at *M1*, and blue crosses correspond to minerals with Mg at *M1*.

approach for individual *M2* and *M3* sites using OccQP (Wright et al., 2000) and the merged-site approach give the same end-member ($M2_2M3$) composition. The empirical $M2_2M3$ compositions for other paulkerrite-group minerals are shown in Fig. 4.

5 Raman spectroscopy

Raman spectroscopy was conducted on a Horiba XploRA PLUS spectrometer using a 532 nm diode laser, 200 μm slit, and 1800 grooves mm^{-1} diffraction grating and a 100 \times (0.9 numerical aperture) objective. The spectrometer was calibrated using the 520.7 cm^{-1} band of silicon. The sample was susceptible to thermal damage at high laser power, so the spectrum was recorded at a laser power of 4 mW. The sample was examined after the spectrum was recorded to verify that no thermal damage had occurred. The spectrum is shown in Fig. 5. The O–H stretch region has a broad band centred at 3460 cm^{-1} with shoulders at 3580, 3460, and 3250 cm^{-1} . The H–O–H bending-mode region for water has a band at 1645 cm^{-1} . The P–O stretching region has a band at 955 cm^{-1} with shoulders at 1005 and 980 cm^{-1} corresponding to symmetric stretching modes and two weaker bands at 1125 and 1077 cm^{-1} corresponding to antisymmetric stretching modes. Bending modes of the $(\text{PO}_4)^{3-}$ groups are manifested by a band centred at 595 cm^{-1} and a pair of

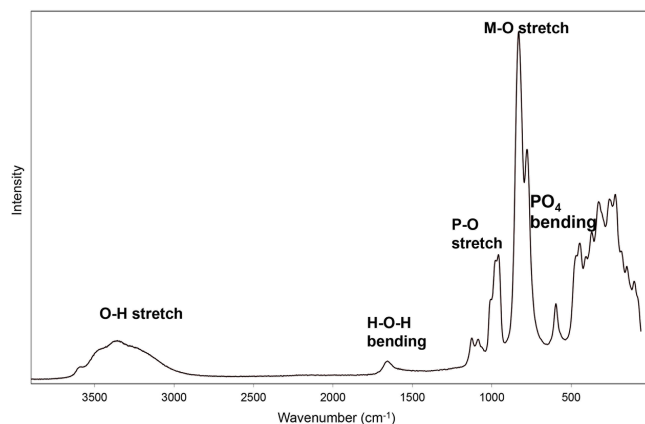


Figure 5. Raman spectrum for macraeite.

bands at 465 and 450 cm^{-1} . Peaks at lower wavenumbers are related to lattice vibrations. An intense pair of bands at 830 and 780 cm^{-1} can be assigned to Ti–O stretch vibrations for short *M2*–O bonds that occur in linear trimers of corner-connected octahedra *M2*–*M3*–*M2* in the structure. The same bands are present in the Raman spectra of all paulkerrite-group minerals that have had spectra reported (Grey et al., 2023b, c, d), and they are consistent with published Raman data for titanates that have short Ti–O distances (Bamberger et al., 1990; Tu et al., 1996; Silva et al., 2018).

6 Crystallography

6.1 X-ray powder diffraction

X-ray powder diffraction data were recorded using a Rigaku R-Axis Rapid II curved-imaging-plate microdiffractometer with monochromatised MoK α radiation. A Gandolfi-like motion on the ϕ and ω axes was used to randomise the sample. Observed *d* values and intensities were derived by profile fitting using JADE Pro software (Materials Data, Inc.). Data are given in Table 2. Refined monoclinic unit-cell parameters (space group $P2_1/c$ (#14)) are $a = 10.56(3)$ \AA , $b = 20.70(3)$ \AA , $c = 12.39(3)$ \AA , $\beta = 90.1(5)^\circ$, $V = 2708(11)$ \AA^3 , and $Z = 4$.

6.2 Synchrotron single-crystal diffraction

A crystal of macraeite measuring 0.10 \times 0.10 \times 0.02 mm was used for a single-crystal diffraction data collection at the Australian Synchrotron microfocus beamline MX2 (Aragao et al., 2018). Intensity data were collected using a Dectris EIGER 16M detector and monochromatic radiation with a wavelength of 0.7109 \AA . The crystal was maintained at 100 K in an open-flow nitrogen cryostream during data collections. The diffraction data were collected using a single 36 s sweep of 360 $^\circ$ rotation around phi. The resulting dataset consists of 3600 individual images with an approximate phi angle of

Table 2. Powder X-ray diffraction data (d in Å) for macraeite ($I_{\text{calc}} > 1.5$).

I_{obs}	d_{obs}	d_{calc}	I_{calc}	hkl	I_{obs}	d_{obs}	d_{calc}	I_{calc}	hkl
94	10.38	10.3485	70	0 2 0			1.9643	2	-5 2 2
64	7.51	7.4890	66	1 1 1			1.9456	4	-4 7 1
		6.3519	2	-1 2 1	19	1.9299	1.9275	4	3 6 4
75	6.25	6.1965	100	0 0 2			1.9183	6	0 4 6
		5.3485	2	-1 0 2	15	1.8809	1.8903	9	2 2 6
		5.2820	19	2 0 0			1.8721	9	5 1 3
50	5.24	5.2373	10	-1 3 1			1.8582	4	2 8 4
		5.1743	15	0 4 0	16	1.8418	1.8404	7	-2 10 2
11	4.73	4.7463	4	1 2 2			1.8193	2	3 5 5
		4.7046	6	2 2 0			1.7881	4	-2 7 5
		4.0166	5	2 0 2	15	1.7867	1.7828	4	-3 0 6
37	3.984	3.9711	30	2 3 1			1.7771	2	4 7 3
		3.7845	3	-1 1 3			1.7356	5	4 6 4
69	3.736	3.7495	47	-2 2 2	24	1.7278	1.7248	11	0 12 0
		3.6963	7	2 4 0			1.7173	3	4 9 1
11	3.435	3.4495	3	0 6 0			1.7024	2	5 7 1
12	3.284	3.3615	5	-1 3 3			1.6931	3	-1 3 7
		3.1759	3	-2 4 2			1.6856	2	-3 4 6
100	3.150	3.1503	58	2 5 1			1.6794	7	2 6 6
		3.0982	26	0 0 4	28	1.6778	1.6739	4	-2 1 7
		3.0595	11	3 0 2			1.6668	10	6 4 0
46	3.030	3.0395	3	3 3 1			1.6616	3	0 12 2
		3.0140	9	0 6 2	20	1.6476	1.6396	2	2 12 0
		2.9718	19	1 0 4			1.6291	5	4 10 0
		2.9449	6	-2 3 3			1.6142	2	0 8 6
67	2.901	2.9339	2	3 2 2	23	1.6137	1.6085	14	-4 2 6
		2.8882	29	2 6 0			1.5997	2	-4 9 3
33	2.849	2.8563	9	1 2 4	15	1.5758	1.5751	7	4 10 2
		2.8189	14	-1 5 3			1.5682	3	6 6 0
		2.6743	6	-2 0 4	8	1.5474	1.5412	4	4 7 5
25	2.655	2.6582	3	0 4 4	12	1.5211	1.5297	3	6 0 4
		2.6362	16	-3 4 2			1.5207	4	4 11 1
		2.6186	15	-2 6 2			1.5070	3	0 12 4
39	2.607	2.5871	5	0 8 0	8	1.4919	1.4998	2	-5 5 5
		2.5770	6	1 4 4			1.4840	6	0 4 8
		2.5639	14	-4 1 1			1.4724	4	-4 6 6
33	2.532	2.5262	14	-2 7 1	18	1.4684	1.4688	5	-6 4 4
		2.4963	6	3 3 3			1.4620	3	0 10 6
8	2.383	2.3874	2	0 8 2			1.4556	2	6 8 0
		2.3757	3	-2 4 4	13	1.4470	1.4494	3	-2 12 4
17	2.340	2.3640	6	4 2 2			1.4425	2	-4 10 4
		2.3284	10	1 8 2	9	1.4183	1.4373	3	4 3 7
		2.2321	2	-2 1 5			1.4094	4	-2 10 6
12	2.200	2.2002	5	-4 4 2	6	1.3908	1.3851	4	3 12 4
		2.1919	3	-4 5 1	3	1.3641	1.3554	4	2 9 7
8	2.130	2.1350	3	-2 3 5	11	1.3326	1.3371	2	-4 0 8
		2.1135	3	-2 6 4			1.3273	6	2 15 1
		2.0970	3	4 6 0	13	1.3118	1.3181	3	-6 8 4
15	2.089	2.0784	4	2 9 1			1.3106	8	-8 1 1
		2.0655	8	0 0 6	4	1.2953	1.2987	2	1 15 3
9	2.018	2.0114	5	-4 0 4	4	1.2787	1.2785	4	4 10 6
34	1.9840	1.9856	21	4 6 2	6	1.2514	1.2549	2	8 1 3

each image being 0.1° . The raw intensity dataset was processed using XDS software to produce data files that were analysed using SHELXT (Sheldrick, 2015) and Jana2006 (Petříček et al., 2014). Refined unit-cell parameters and other data collection details are given in Table 3.

A structural model for macraeite was obtained in space group $P2_1/c$ using SHELXT (Sheldrick, 2015). The model was found to have the same topology as for rewitzerite (Grey et al., 2023b), so the rewitzerite atom coordinates were used as a starting model to maintain the same atom labelling. Twinning was implemented with 2-fold rotation about [001]. The general structural formula for monoclinic paulkerrite-group members may be written as $A1A2M1_2M2_2M3(PO_4)_4X_2(H_2O)_{10} \cdot 4H_2O$ (Grey et al., 2023a). Manganese, Fe, and Ti were assigned as site scatterers to the $M1$, $M2$, and $M3$ sites, respectively; their occupation factors were refined; and a mix of K and O (for H_2O) was assigned to the $A1$ and $A2$ sites. After refinement the M -site scattering values were used in OccQP (Wright et al., 2000) to optimise the site assignments. This showed that minor elements Al and Mg were confined to the $M2$ sites with Fe and Ti, while only Fe and Ti were at the $M3$ sites. In the next stage of the refinement, the amount of Al from the EMP analyses was allocated to the $M2$ sites and fixed, while the Ti and Fe contents were refined at the $M2$ and $M3$ sites. Approximately two-thirds of the possible H atoms were located in difference Fourier maps. Their positions were included in the atom list but not refined. Refinement of all non-H atoms with anisotropic displacement parameters and with a group isotropic displacement parameter for the H atoms, in Jana2006 (Petříček et al., 2014), converged at $R_{obs} = 0.047$ for 4979 reflections with $I > 3\sigma(I)$.

Details of the data collection and refinement are given in Table 3. The refined coordinates, equivalent isotropic displacement parameters, and bond valence sum (BVS) values (Gagné and Hawthorne, 2015) from the single-crystal refinement are reported in Table 4. Selected interatomic distances are reported in Table 5, and H bonds are given in Table 6.

6.3 Laboratory single-crystal diffraction

A diffraction dataset was collected at 300 K using an XtaLAB Synergy four-circle diffractometer equipped with a Dualflex HyPix detector and using $MoK\alpha$ radiation. Processing of the data using CrysAlisPro (Rigaku, 2022) gave the monoclinic unit-cell parameters $a = 10.5383(4)$ Å, $b = 20.7316(7)$ Å, $c = 12.4658(5)$ Å, and $\beta = 90.144(5)^\circ$. The structure was refined using the same procedure as described for the synchrotron dataset in Sect. 6.2, with the published atomic coordinates for rewitzerite (Grey et al., 2023b) as starting coordinates. Refinement with isotropic displacement parameters using Jana2006 converged at $R_{obs} = 0.078$ for 3163 reflections with $I > 3\sigma(I)$ and gave the refined occupancies at the A sites as $0.12(1)K + 0.88O$ at $A1$ and $0.75(2)K + 0.25O$ at $A2$, similar to values obtained from

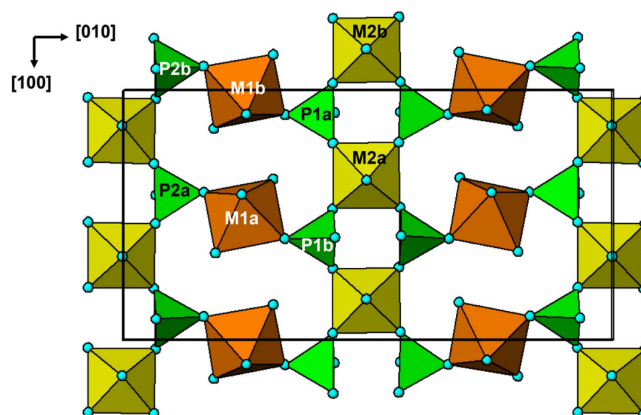


Figure 6. The (001) section through the macraeite crystal structure at $z = 1/4$.

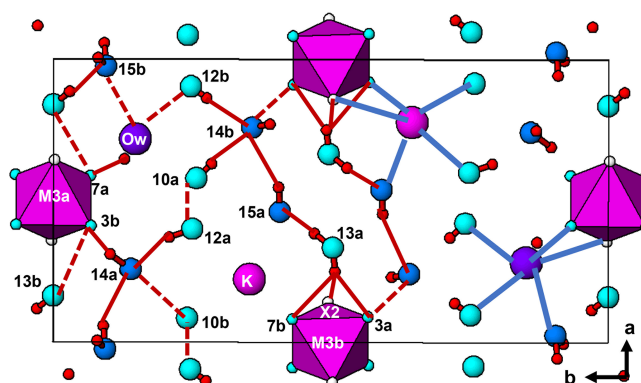


Figure 7. The (001) section through the macraeite structure at $z = 0$. On the left-hand side of the figure, H bonding involving located H atoms (Table 6) is shown by solid red lines and inferred H bonding based on $O \cdots O$ separations is shown by dotted lines. On the right-hand side, the in-section bonds to $A1$ and $A2$ are shown by the blue lines.

the synchrotron data refinement (Table 4). Attempts to refine with anisotropic displacement parameters were not successful, resulting in several non-positive values, and H atoms could not be unambiguously located in difference Fourier maps, so the following discussion will refer to the synchrotron data refinement results. The laboratory-based single-crystal study, however, confirmed that macraeite has monoclinic symmetry at ambient temperature and is not due to a transition from the orthorhombic $Pbca$ benyacarite-type structure (Demartin et al., 1993) to monoclinic $P2_1/c$ type at below room temperature.

Table 3. Crystal data and structure refinement for macraeite.

End-member formula	$[(\text{H}_2\text{O})\text{K}]\text{Mn}_2(\text{Fe}_2\text{Ti})(\text{PO}_4)_4[\text{O}(\text{OH})](\text{H}_2\text{O})_{10} \cdot 4\text{H}_2\text{O}$
Formula weight	991.46
Temperature	100 K
Wavelength	0.7107 Å
Space group	$P2_1/c$ (#14)
Unit-cell dimensions	$a = 10.562(2)$ Å $b = 20.725(4)$ Å $c = 12.416(2)$ Å $\beta = 90.09(3)^\circ$
Volume	$2717.8(9)$ Å ³
Z	4
Absorption correction	Multiscan, $\mu = 2.74 \text{ mm}^{-1}$ $T_{\text{min}} 0.563$, $T_{\text{max}} 0.746$
Twinning	2-fold rotation about c Twin vols. 0.367(3), 0.633
Crystal size	$0.10 \times 0.10 \times 0.02$ mm
Theta range for data collection	1.91 to 31.95°
Index ranges	$-14 \leq h \leq 14$, $-27 \leq k \leq 27$, $-17 \leq l \leq 17$
Reflections collected	49 554
Independent reflections	5296 ($R_{\text{merge}} = 0.035$)
Reflections with $I_0 > 3\sigma(I)$	4990
Refinement method	Full-matrix least squares on F
Data/restraints/parameters	5296/0/376
Final R indices [$I > 3\sigma(I)$]	$R_{\text{obs}} = 0.047$, $wR_{\text{obs}} = 0.063$
R indices (all data)	$R_{\text{obs}} = 0.049$, $wR_{\text{obs}} = 0.064$
Largest diff. peak and hole	1.13 and $-1.52 e \text{ \AA}^{-3}$

7 Discussion

Macraeite is isostructural with paulkerrite (Grey et al., 2023a) and rewitzerite (Grey et al., 2023b). The structures of the three minerals correspond to small distortions of the orthorhombic benyacarite $Pbca$ structure (Demartin et al., 1993). In the monoclinic $P2_1/c$ structures, the $Pbca$ atom sites are each split into pairs of sites at x , y , z and $1/2 + x$, $1/2 - y$, $-z$. The A -site constituents, K and H_2O , are ordered in separate $A1$ and $A2$ sites in the monoclinic minerals, whereas they are disordered at a single A site in orthorhombic benyacarite. In contrast to the A -site ordering, there are only minor variations in the compositions between the pairs of M sites in the monoclinic structures. In particular, the compositions at the pairs of $M1$ and $M2$ sites in all three monoclinic minerals are the same within experimental

error. There is, however, a reasonably strong site preference for Ti at the $M3a$ sites and trivalent cations Fe^{3+} and Al^{3+} at the $M3b$ site as shown by the $M3a$ and $M3b$ site occupancies and BVS values for macraeite in Table 4. The same preference of Ti for the $M3a$ site was found for paulkerrite (Grey et al., 2023a).

The crystal structure of the paulkerrite-group minerals is quite complex and can be described in different ways that give emphasis to different features (Demartin et al., 1993; Grey et al., 2023a, b). The most general description, using the terminology of Hawthorne (Hawthorne, 1992; Hawthorne and Schindler, 2008), is in terms of a structural unit plus an interstitial complex. For macraeite, the structural unit is a 3D anionic framework of corner-connected octahedra and tetrahedra, with composition $[\text{Mn}_2(\text{Fe}_2^{3+}\text{Ti})(\text{PO}_4)_4[\text{O}(\text{OH})](\text{H}_2\text{O})_{10}]^{1-}$, while the in-

Table 4. Refined atom coordinates, equivalent isotropic displacement parameters (\AA^2), and bond valence sums (BVSs, in valence units) for macraeite.

Site	x	y	z	U_{eq}	BVS
M1a	0.49453(5)	0.74657(3)	0.24480(4)	0.02077(15)	2.09
M1b	0.99609(5)	-0.24686(3)	-0.24286(4)	0.02077(15)	2.08
M2a	0.66057(7)	0.50265(3)	0.74639(5)	0.01990(12)	3.32
M2b	1.16022(7)	-0.00248(3)	-0.74466(5)	0.01990(12)	3.18
M3a	0.5	0.5	0.5	0.02132(14)	4.02
M3b	1	0	-0.5	0.02132(14)	3.54
P2a	0.58649(11)	0.59045(5)	0.29502(8)	0.0181(3)	4.94
P2b	1.08635(11)	-0.09074(4)	-0.29605(8)	0.0189(3)	5.01
P1a	0.90731(11)	0.59515(4)	0.80124(8)	0.0183(3)	4.96
P1b	1.40878(11)	-0.09538(4)	-0.80260(8)	0.0185(3)	4.96
A1	0.7173(2)	0.85227(9)	0.05951(15)	0.0287(7)	0.80*
A2	1.22219(13)	-0.35395(5)	-0.05701(10)	0.0279(4)	0.86*
X1	0.6416(3)	0.50268(10)	0.5965(3)	0.0187(4)	1.41
X2	1.1429(3)	-0.00392(10)	-0.5959(3)	0.0187(4)	1.36
O1a	0.9040(3)	0.66903(11)	0.8064(2)	0.0223(8)	1.69
O1b	1.4024(3)	-0.16825(12)	-0.8049(2)	0.0225(8)	1.75
O2a	1.0251(3)	0.57228(13)	0.7374(2)	0.0178(8)	1.62
O2b	1.5269(3)	-0.07182(13)	-0.7408(2)	0.0239(9)	1.66
O3a	0.9101(3)	0.56781(13)	0.9147(2)	0.0236(8)	1.86
O3b	1.4103(3)	-0.06799(12)	-0.9194(2)	0.0215(7)	1.82
O4a	0.7857(3)	0.57196(13)	0.7426(2)	0.0219(8)	1.74
O4b	1.2872(3)	-0.07114(13)	-0.7470(2)	0.0209(8)	1.82
O5a	0.5955(3)	0.66352(12)	0.2909(2)	0.0219(8)	1.72
O5b	1.0947(3)	-0.16405(12)	-0.2906(2)	0.0243(8)	1.72
O6a	0.4652(3)	0.56718(13)	0.2371(3)	0.0234(9)	1.70
O6b	0.9684(3)	-0.06696(13)	-0.2346(2)	0.0192(8)	1.69
O7a	0.5860(3)	0.56674(12)	0.4131(2)	0.0206(7)	1.87
O7b	1.0815(3)	-0.06882(13)	-0.4125(2)	0.0234(8)	1.96
O8a	0.7061(3)	0.56331(13)	0.2387(2)	0.0207(8)	1.71
O8b	1.2068(3)	-0.06296(13)	-0.2406(2)	0.0227(9)	1.70
O9a	0.3450(3)	0.68463(13)	0.1771(2)	0.0297(9)	0.36
O9b	0.8470(3)	-0.18619(13)	-0.1763(3)	0.0294(9)	0.35
O10a	0.5791(3)	0.74226(13)	0.0782(3)	0.0264(8)	0.32
O10b	1.0839(3)	-0.24177(13)	-0.0763(3)	0.0292(9)	0.39
O11a	0.6426(3)	0.80781(13)	0.3136(3)	0.0284(8)	0.35
O11b	1.1469(3)	-0.30876(13)	-0.3057(3)	0.0303(9)	0.36
O12a	0.3997(3)	0.75071(13)	0.4066(3)	0.0278(8)	0.38
O12b	0.9033(3)	-0.25244(13)	-0.4076(3)	0.0267(8)	0.30
O13a	0.6656(3)	0.50382(11)	0.9129(3)	0.0249(9)	0.38
O13b	1.1624(4)	-0.00022(11)	-0.9184(3)	0.0262(10)	0.30
O14a	0.2572(3)	0.63990(13)	0.44072(19)	0.0288(9)	0.00
O14b	0.7582(3)	-0.14179(14)	-0.4413(2)	0.0317(9)	0.00
O15a	0.5400(4)	0.40855(14)	1.0164(2)	0.0390(10)	0.10
O15b	1.0248(3)	0.09439(16)	-1.0100(2)	0.0402(10)	0.02
Ha1a	0.647	0.8709	0.0083	0.072(4)	
H9a1	0.2531	0.6963	0.1891	0.072(4)	
H9a2	0.387	0.6395	0.1932	0.072(4)	
H9b1	0.8799	-0.1305	-0.182	0.072(4)	
H9b2	0.7464	-0.1909	-0.176	0.072(4)	
H10a1	0.6302	0.7154	0.0726	0.072(4)	
H11a1	0.7285	0.8049	0.3089	0.072(4)	
H11a2	0.6101	0.8508	0.2894	0.072(4)	
H11b1	1.2387	-0.2997	-0.3054	0.072(4)	
H11b2	1.1357	-0.3556	-0.2891	0.072(4)	
H12a1	0.3699	0.7086	0.4104	0.072(4)	
H12b1	0.864	-0.2215	-0.4107	0.072(4)	
H13a1	0.6188	0.4736	0.953	0.072(4)	
H13a2	0.747	0.5074	0.931	0.072(4)	
H13b2	1.1141	0.0308	-0.9549	0.072(4)	
H14a1	0.2493	0.6233	0.3917	0.072(4)	
H14a2	0.3106	0.606	0.4915	0.072(4)	
H14b1	0.7722	-0.1082	-0.3938	0.072(4)	
H15a1	0.4529	0.4058	0.9827	0.072(4)	
H15b1	0.9968	0.0809	-1.087	0.072(4)	
H15b2	0.9462	0.0908	-0.9729	0.072(4)	

M1a = Mn, M1b = 0.985(4)Mn, M2a = 0.15A1 + 0.70(2)Fe + 0.15(2)Ti,
M2b = 0.15A1 + 0.67(2)Fe + 0.18(2)Ti, M3a = 0.99(2)Ti + 0.01(2)Fe, M3b = 0.32(2)Ti + 0.68(2)Fe,
A1 = 0.174(6)K + 0.826(6)O, and A2 = 0.650(6)K + 0.350(6)O. * BVS for A1 and A2 based on full
occupation by K.

Table 5. Polyhedral bond lengths [\AA] for macraeite.

<i>M1a</i>	– O1b	2.108(3)	<i>M1b</i>	– O1a	2.088(3)
	– O5a	2.104(3)		– O5b	2.094(3)
	– O9a	2.201(3)		– O9b	2.179(3)
	– O10a	2.256(3)		– O10b	2.268(4)
	– O11a	2.187(3)		– O11b	2.190(3)
	– O12a	2.248(3)		– O12b	2.270(3)
Avg		2.184	Avg		2.181
<i>M2a</i>	– X1	1.872(3)	<i>M2b</i>	– X2	1.856(3)
	– O2b	2.018(3)		– O2a	2.044(3)
	– O4a	1.953(3)		– O4b	1.955(3)
	– O6a	1.975(3)		– O6b	1.996(3)
	– O8b	1.954(3)		– O8a	1.964(3)
	– O13a	2.068(4)		– O13b	2.158(3)
Avg		1.973	Avg		1.995
<i>M3a</i>	– X1 \times 2	1.915(3)	<i>M3b</i>	– X2 \times 2	1.926(3)
	– O3b \times 2	1.971(3)		– O3a \times 2	1.999(3)
	– O7a \times 2	1.976(3)		– O7b \times 2	1.989(3)
Avg		1.954	Avg		1.971
<i>P1a</i>	– O1a	1.533(3)	<i>P1b</i>	– O1b	1.512(3)
	– O2a	1.550(3)		– O2b	1.543(3)
	– O3a	1.519(3)		– O3b	1.558(3)
	– O4a	1.551(3)		– O4b	1.543(3)
Avg		1.538	Avg		1.539
<i>P2a</i>	– O5a	1.518(3)	<i>P2b</i>	– O5b	1.524(3)
	– O6a	1.546(3)		– O6b	1.543(3)
	– O7a	1.546(3)		– O7b	1.516(3)
	– O8a	1.551(3)		– O8b	1.556(3)
Avg		1.540	Avg		1.535
<i>A1</i>	– X1	3.145(3)	<i>A2</i>	– X2	3.100(3)
	– O4a	2.855(4)		– O4b	2.907(3)
	– O7a	2.835(4)		– O7b	2.828(3)
	– O9b	3.331(4)		– O9a	3.280(4)
	– O10a	2.718(4)		– O10b	2.756(3)
	– O11a	3.382(4)		– O11b	3.322(4)
	– O12b	2.882(4)		– O12a	2.881(3)
	– O15b	3.003(4)		– O15a	2.800(4)
Avg		3.019	Avg		2.984

terstitial complex is $[\text{K}(\text{H}_2\text{O})(\text{H}_2\text{O})_4]^{1+}$, where the first H_2O (transformer type; Hawthorne, 1992) corresponds to O15a coordinated to K at A2 and the four other H_2O are involved only in H bonding. These comprise O14a, O14b, O15b, and A1 in Table 4. The structural unit is built from (001) heteropolyhedral layers, $M_1M_2M_2(\text{PO}_4)_4X_2(\text{H}_2\text{O})_{10}$, centred at $z = 1/4$ and $3/4$. The layer at $z = 1/4$ is shown in Fig. 6. The layers contain [100] kröhnkite-type chains (Hawthorne, 1985) of four-member rings of corner-connected PO_4 tetrahedra and $M_2\text{O}_4X(\text{H}_2\text{O})$ octahedra. Each PO_4 tetrahedron also shares a corner with $M_1\text{O}_2(\text{H}_2\text{O})_4$ octahedra along

[010]. The corner-shared linkages form eight-member rings of alternating octahedra and tetrahedra. Layers as shown in Fig. 6 are interconnected into an open 3D framework (the structural unit) by corner sharing of the $M_2\text{O}_4X(\text{H}_2\text{O})$ octahedra with $M_3\text{O}_4X_2$ octahedra located at $z = 0$ and $1/2$.

The interstitial complex is located in (100) sections centred at $z = 0$ and $1/2$. The section at $z = 0$ is shown in Fig. 7. In addition to the interstitial constituents, the section contains isolated $M_3\text{O}_4X_2$ octahedra and water molecules coordinated to *M1* (O10 and O12) and to *M2* (O13). Rows of uniformly spaced water molecules are oriented along $\langle 110 \rangle$.

Table 6. H bonds in macraeite.

D–H–A	D–H (Å)	H···A (Å)	D···A (Å)	D–H···A (°)
O9a–H9a1–O5b	1.012(3)	1.819(3)	2.708(5)	144.63(17)
O9a–H9a2–O6a	1.055(3)	1.795(3)	2.844(4)	172.47(19)
O9b–H9b1–O6b	1.206(3)	1.744(3)	2.877(4)	154.01(17)
O9b–H9b2–O5a	1.067(3)	1.740(3)	2.727(4)	151.73(17)
O10a–H10a1–O14b	0.778(3)	2.047(3)	2.824(4)	177.4(2)
O11a–H11a1–O1a	0.911(3)	1.931(3)	2.803(5)	159.71(18)
O11a–H11a2–O2b	1.002(3)	1.866(3)	2.859(4)	170.5(2)
O11b–H11b1–O1b	0.987(3)	1.853(3)	2.741(5)	148.11(18)
O11b–H11b2–O2a	0.999(3)	1.926(3)	2.832(4)	149.4(2)
O11b–H11b2–O4b	0.999(3)	2.266(3)	2.986(4)	128.0(2)
O12a–H12a1–O14a	0.929(3)	1.894(3)	2.779(4)	158.3(2)
O12b–H12b1–O14b	0.765(3)	2.029(3)	2.789(4)	172.0(3)
O13a–H13a1–O15a	0.941(3)	1.770(3)	2.704(4)	172.0(2)
O13a–H13a2–X2	0.892(4)	2.365(3)	3.044(5)	133.0(2)
O13a–H13a2–O3a	0.892(4)	2.138(3)	2.903(5)	143.34(19)
O13a–H13a2–O7b	0.892(4)	2.415(3)	3.066(5)	130.10(18)
O13b–H13b2–O15b	0.936(3)	1.759(3)	2.691(5)	173.4(2)
O14a–H14a1–O8b	0.704(2)	2.112(3)	2.809(4)	170.5(2)
O14a–H14a2–O3b	1.100(3)	1.717(3)	2.801(4)	167.54(17)
O14b–H14b1–X2	0.925(3)	2.493(2)	3.228(4)	136.6(2)
O14b–H14b1–O8a	0.925(3)	2.015(3)	2.819(4)	144.4(2)
O15a–H15a1–O14b	1.012(4)	2.491(3)	3.446(5)	157.07(18)
O15b–H15b1–O2a	1.038(3)	1.890(3)	2.908(4)	165.8(2)
O15b–H15b1–O13b	1.038(3)	2.372(3)	2.916(5)	111.4(2)
O15b–H15b2–O14a	0.953(3)	2.411(3)	3.242(5)	145.5(2)
A1–HA1a–O7a	1.050(2)	1.866(3)	2.835(4)	151.79(15)

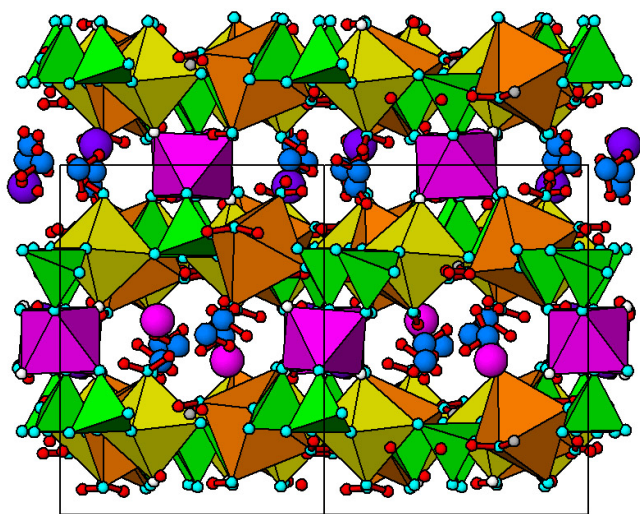


Figure 8. The $\langle 110 \rangle$ projection of the crystal structure of macraeite showing channels containing the interstitial constituents. The c axis [001] is vertical. The coloured polyhedra are as labelled in Figs. 6 and 7.

A $\langle 110 \rangle$ projection of the crystal structure in Fig. 8 shows that the interstitial species occupy $\langle 110 \rangle$ channels in the structural unit. The H bonding involving the H atoms located in the refinement is given in Table 6. Libowitzky (1999) has classified H bonds according to the donor–acceptor separation as being strong for donor–acceptor distances in the range 2.50 to 2.70 Å and weak for distances above 2.70 Å. In macraeite, only O9, coordinated to $M1$, and O13, coordinated to $M2$, are donors that participate in strong H bonds. Most of the bonds are from water molecules to oxygen atoms O1 to O8, shared between M -centred octahedra and PO_4 tetrahedra. As seen from the BVS values in Table 4, these bridging oxygens are all undersaturated with BVS values typically from 1.7 to 1.8, and their bond valence saturation is met by them being acceptor atoms for H bonds. Additionally there are in-section bonds between coordinated water molecules of the structural unit and those of the interstitial complex, the strongest being from O13, coordinated to $M2$, and O15. The O13 molecules have trifurcated H bonds to anions X, O3, and O7, which form a face of the $M3$ -centred octahedra, shown in Fig. 7. In addition, O11, O14, and O15 act as donors forming bifurcated H bonds as given in Table 6.

The in-section coordination of the constituents at the A1 and A2 sites is shown in Fig. 7, and their complete (8-fold) coordination is given in Table 5. The coordination polyhedra

Table 7. Comparison of rewitzerite and macraeite.

	Rewitzerite	Macraeite
Ideal formula	$\text{K}(\text{H}_2\text{O})\text{Mn}_2(\text{Al}_2\text{Ti})(\text{PO}_4)_4[\text{O}(\text{OH})](\text{H}_2\text{O})_{10} \cdot 4\text{H}_2\text{O}$	$[(\text{H}_2\text{O})\text{K}]\text{Mn}_2(\text{Fe}_2\text{Ti})(\text{PO}_4)_4[(\text{O}(\text{OH}))_2(\text{H}_2\text{O})_{10} \cdot 4\text{H}_2\text{O}]$
Crystal system	monoclinic	monoclinic
Space group	$P2_1/c$	$P2_1/c$
a (Å)	10.444(2)	10.562(2)
b (Å)	20.445(2)	20.725(4)
c (Å)	12.2690(12)	12.416(2)
β (°)	90.17(3)	90.09(3)
V (Å ³)	2619.8(6)	2717.8(9)
Z	4	4
Strongest lines in	10.26 (53) (020) 7.44 (55) (−111)	10.38 (94) (020) 7.51 (64) (111)
X-ray powder pattern	6.16 (92) (002) 5.19 (40) (200) 3.958 (32) (−231)	6.25 (75) (002) 5.24 (50) (200, −131) 3.984 (37) (231)
D (l) (hkl)	3.703 (57) (−222) 3.111 (97) (−251) 2.862 (100) (260)	3.736 (69) (−222) 3.150 (100) (251) 2.901 (67) (260)
Dcalc (g cm ^{−3})	2.33	2.39
Opt. character	biaxial (+)	biaxial (+)
α	1.585(2)	1.605(3)
β	1.586(2)	1.611(3)
γ	1.615(2)	1.646(3)
$2V_{\text{meas}}$ (°)	25(2)	45(3)
Reference	Grey et al. (2023b)	this study

for the two sites are very similar with the mean A–O distance differing by only 0.035 Å. The major difference is associated with the water molecule O15, which is 0.2 Å closer to the K-dominant A2 site than to the H₂O-dominant A1 site. The factors determining the ordering of K at one A site and H₂O at the other are very subtle and probably depend as much on establishing the most favourable H bonding as on locally matching the structural unit's negative charge because the large 8-coordinated K⁺ has a low bond valence of 0.125, comparable to bond valence contributions from the medium- to weak-strength H bonds listed in Table 6. The K ordering in macraeite is far from full ordering; with 0.17 K at A1 and 0.65 K at A2, this corresponds to a mixture of 60 % full order (0.82 K at A2) + 40 % complete disorder (0.41 K at A1 and A2). The low degree of A-site order reflects the low degree of ordering of trivalent and tetravalent cations at the M2 and M3 sites of the structural unit.

Data availability. Crystallographic data for macraeite are available in the Supplement.

Supplement. The supplement related to this article is available online at: <https://doi.org/10.5194/ejm-36-267-2024-supplement>.

Author contributions. IEG oversaw the research and wrote the paper. CR field-collected the specimen. RH and CR obtained preliminary EDS analyses, and CR obtained optical images of the specimen. WGM assisted in the diffraction data analysis. ARK measured the optical properties, Raman spectrum, powder XRD, and crystal morphology. SB collected and processed the single-crystal diffraction data, and NCW performed the site assignment analysis.

Competing interests. The contact author has declared that none of the authors has any competing interests.

Disclaimer. Publisher's note: Copernicus Publications remains neutral with regard to jurisdictional claims made in the text, published maps, institutional affiliations, or any other geographical representation in this paper. While Copernicus Publications makes every effort to include appropriate place names, the final responsibility lies with the authors.

Acknowledgements. We thank Cameron Davidson for preparing polished mounts for EMP analyses. Thanks go to Robert Gable for collecting and processing the laboratory-based single-crystal diffraction results. This research was undertaken in part using the MX2 beamline at the Australian Synchrotron, part of ANSTO, and made use of the Australian Cancer Research Foundation Detector.

Review statement. This paper was edited by Sergey Krivovichev and reviewed by Sergey Britvin and Lyudmila Lyalina.

References

- Aragao, D., Aishima, J., Cherukuvada, H., Clarken, R., Clift, M., Cowieson, N. P., Ericsson, D. J., Gee, C. L., Macedo, S., Mudie, N., Panjekar, S., Price, J. R., Riboldi-Tunnicliffe, A., Rostan, R., Williamson, R., and Caradoc-Davies, T. T.: MX2: a high-flux undulator microfocus beamline serving both the chemical and macromolecular crystallography communities at the Australian Synchrotron, *J. Synch. Radiat.*, 25, 885–891, 2018.
- Bamberger, C. E., Begun, G. M., and MacDougall, C. S.: Raman spectroscopy of potassium titanates: Their synthesis, hydrolytic reactions and thermal stability, *Appl. Spectrosc.*, 44, 31–37, 1990.
- Bosi, F., Hatert, F., Halenius, U., Pasero, M., Ritsuro, M., and Mills, S. J.: On the application of the IMA-CNMNC dominant-valency rule to complex mineral compositions, *Mineral. Mag.*, 83, 627–632, 2019a.
- Bosi, F., Biagioni, C., and Oberti, R.: On the chemical identification and classification of minerals, *Minerals*, 9, 591, <https://doi.org/10.3390/min9100591>, 2019b.
- Demartin, F., Pilati, T., Gay, H. D., and Gramaccioli, C. M.: The crystal structure of a mineral related to paulkerrite, *Z. Kristallogr.*, 208, 57–71, 1993.
- Demartin, F., Gay, H. D., Gramaccioli, C. M., and Pilati, T.: Benyacarite, a new titanium-bearing phosphate mineral species from Cerro Blanco, Argentina, *Can. Mineral.*, 35, 707–712, 1997.
- Fransolet, A.-M., Oustriere, P., Fontan, F., and Pillard, F.: La mantienneite, une nouvelle espèce minérale du gisement de vivianite d'Anloua, Cameroun. *Bull. Mineral.*, 107, 737–744, 1984.
- Gagné, O. C. and Hawthorne, F. C.: Comprehensive derivation of bond-valence parameters for ion pairs involving oxygen, *Acta Crystallogr. B*, 71, 562–578, 2015.
- Grey, I. E., Boer, S., MacRae, C. M., Wilson, N. C., Mumme, W. G., and Bosi, F.: Crystal chemistry of type paulkerrite and establishment of the paulkerrite group nomenclature, *Eur. J. Mineral.*, 35, 909–919, <https://doi.org/10.5194/ejm-35-909-2023>, 2023a.
- Grey, I. E., Hochleitner, R., Kampf, A. R., Boer, S., MacRae, C. M., Mumme, W. G., and Keck, E.: Rewitzerite, $[K(H_2O)]Mn_2(Al_2Ti)(PO_4)_4[O(OH)](H_2O)_{10} \cdot 4H_2O$, a new monoclinic paulkerrite-group mineral, from the Hagendorf Süd pegmatite, Oberpfalz, Bavaria, Germany, *Mineral. Mag.*, 87, 830–838, 2023b.
- Grey, I. E., Hochleitner, R., Rewitzer, C., Kampf, A. R., MacRae, C. M., Gable, R. W., Mumme, W. G., Keck, E., and Davidson, C.: Pleysteinite, $[(H_2O)_{0.5}K_{0.5}]_2Mn_2Al_3(PO_4)_4F_2(H_2O)_{10} \cdot 4H_2O$, the Al analogue of benyacarite, from the Hagendorf-Süd pegmatite, Oberpfalz, Bavaria, Germany, *Eur. J. Mineral.*, 35, 189–197, <https://doi.org/10.5194/ejm-35-189-2023>, 2023c.
- Grey, I. E., Keck, E., Kampf, A. R., MacRae, C. M., Gable, R. W., Mumme, W. G., Wilson, N. C., Glenn, A. M., and Davidson, C.: Hochleitnerite, $[K(H_2O)]Mn_2(Ti_2Fe)(PO_4)_4O_2(H_2O)_{10} \cdot 4H_2O$, a new paulkerrite-group mineral, from the Hagendorf-Süd pegmatite, Oberpfalz, Bavaria, Germany, *Eur. J. Mineral.*, 35, 635–643, <https://doi.org/10.5194/ejm-35-635-2023>, 2023d.
- Gunter, M. E., Bandli, B. R., Bloss, F. D., Evans, S. H., Su, S. C., and Weaver, R.: Results from a McCrone spindle stage short course, a new version of EXCALIBUR, and how to build a spindle stage, *The Microscope*, 52, 23–39, 2004.
- Hawthorne, F. C.: Towards a structural classification of minerals: The $^{vi}M^{iv}T_2\Phi_n$ minerals, *Am. Mineral.*, 70, 455–473, 1985.
- Hawthorne, F. C.: The role of OH and H₂O in oxide and oxysalt minerals, *Z. Krist.*, 201, 41–68, 1992.
- Hawthorne, F. C. and Schindler, M.: Understanding the weakly bonded constituents in oxysalt minerals, *Z. Krist.*, 223, 183–206, 2008.
- Keck, E., Witzke, T., Pollmann, H., and Friese, K.: Benyacarite aus ostbayrischen und portugiesischen Pegmatiten, *Aufschluss*, 49, 281–285, 1998.
- Libowitzky, E.: Correlation of O-H stretching frequencies and O-H...O hydrogen bond lengths in minerals, *Monatsch. Chemie*, 130, 1047–1059, 1999.
- Mandarino, J. A.: The Gladstone-Dale relationship: Part IV, The compatibility concept and its application, *Can. Mineral.*, 19, 441–450, 1981.
- Peacor, D. R., Dunn, P. J., and Simmons, W. B.: Paulkerrite a new titanium phosphate from Arizona, *Mineral. Rec.*, 15, 303–306, 1984.
- Petříček, V., Dušek, M., and Palatinus, L.: Crystallographic Computing System JANA2006: General features, *Z. Kristallogr.*, 229, 345–352, 2014.
- Rigaku OD: CrysAlisPro 1.171.42.72a, 2022.
- Schnorrer, G. and Tetzer, G.: Paulkerrite, $K(Mg,Mn)_2Fe_2Ti[(OH)_3(PO_4)_4 \cdot 15H_2O$ von Folgoso in Portugal, ein weiterer Fundort fuer diese seltene Verbindung, *Aufschluss*, 56, 258–260, 2005.
- Sejkora, J., Skoda, R., Ondrus, P., Beran, P., and Susser, C.: Mineralogy of phosphate accumulations in the Huber stock, Krasno ore district, Slavkovsky les area, Czech Republic, *J. Czech geol. Soc.*, 51, 103–147, 2006.
- Sheldrick, G. M.: Crystal structure refinement with SHELXL, *Acta Crystallogr. C*, 71, 3–8, 2015.
- Silva, F. L. R., Filho, A. A. A., Silva, M. B., Balzuweit, K., Banti-gnies, J.-L., Caetano, E. W. S., Moreira, R. L., Freire, V. N., and Righi, A.: Polarized Raman, FTIR, and DFT study of Na₂Ti₃O₇ microcrystals, *J. Raman Spectrosc.*, 49, 535–548, 2018.
- Tu, C.-S., Guo, A. R., Tao, R., Katiyar, R. S., Guo, R., and Bhalla, A. S.: Temperature dependent Raman scattering in KTiOPO₄ and KTiOAsO₄ single crystals, *J. Appl. Phys.*, 79, 3235–3240, 1996.
- Wright, S. E., Foley, J. A., and Hughes, J. M.: Optimisation of site occupancies in minerals using quadratic programming, *Am. Mineral.*, 85, 524–531, 2000.